Highly sensitive and tunable detection of far-infrared radiation by quantum Hall devices

Y. Kawano,[a] Y. Hisanaga,[b] H. Takenouchi,[c] and S. Komiyama
Department of Basic Science, University of Tokyo, Komaba 3-8-1, Meguro-ku, Tokyo 153-8902, Japan

(Received 2 June 2000; accepted for publication 5 January 2001)

We studied far-infrared (FIR) response due to cyclotron resonance (CR) of two-dimensional electron gas systems in GaAs/AlGaAs heterostructures by using cyclotron radiation from *n*-InSb devices as the illumination source. We examined the dependence of the FIR response on different experimental parameters, including the aspect ratio of Hall bars, electron mobility, bias current, illumination intensity, magnetic field, and lattice temperature. A strong photoresponse emerges only in the vicinity of integer quantum Hall effect (IQHE) regimes. Time-resolved measurements show that the recombination lifetime of excited carriers depends largely on the electron mobility, ranging from 5 μs to 1 ms at 4.2 K. The temporal decay of photoresponse is nonexponential in higher-mobility samples, whereas it is exponential with a single time constant in lower-mobility samples. This, together with the relatively large time constants, suggests that the FIR response is induced through multitrapping processes, in which excited carriers in Landau levels are repeatedly captured by localized states and reexcited to delocalized states. This multitrapping process is suggested to be promoted by the CR-induced heating of the electron system. Theoretical calculation based on the electron heating model reasonably reproduces characteristic dependence of the photoresponse on the magnetic field in the vicinity of IQHE plateaus. The IQHE Hall bars serve as a high-sensitive narrow-band FIR detector, where the highest sensitivity reaches $\sim 10^8$ V/W. Tunability of the detector is demonstrated by varying the electron density. We discuss briefly the design of high-sensitive FIR detectors using the IQHE Hall bars. [DOI: 10.1063/1.1352685]

I. INTRODUCTION

When an integer number, ν, of Landau levels formed in two-dimensional electron gas (2DEG) systems is completely filled with electrons at high magnetic fields, the longitudinal resistance, R_{xx}, of a 2DEG layer vanishes while the Hall resistance, R_H, is quantized to a value $(h/e^2)/\nu$ at low temperatures.[1,2] The exact quantization of R_H, well known as the integer quantum Hall effect (IQHE), has found its use as a resistance standard. The other unique property, $R_{xx}=0$, makes the IQHE device a promising candidate for an excellent detector of far-infrared (FIR) radiation.

When a Hall bar device in the IQHE state is illuminated with FIR radiation of the photon energy equal to the Landau level energy spacing, electrons and holes are excited via cyclotron resonance (CR) in Landau levels above and below the Fermi level. The excited nonequilibrium carriers lead to a dissipative photocurrent, which yields nonvanishing longitudinal resistivity, $\Delta\rho_{xx}$. In a given Hall bar under a given illumination intensity, therefore, a photoresponse signal

$$V_{\mathrm{sig}}=\Delta V_{xx}=\Delta R_{xx}I=(L/W)\Delta\rho_{xx}I, \tag{1}$$

will be induced, where I is the bias current, W is the width of the Hall bar, and L is the device length over which V_{sig} is studied. The induced $\Delta\rho_{xx}$ may be proportional to the incident power density of radiation, $i=\partial P_{\mathrm{FIR}}/\partial A$, with A being the unit area. Therefore, if the active detector area, $S=LW$, is kept unchanged so that the 2DEG absorbs a constant FIR power $\Delta P_{\mathrm{FIR}}=Si$, the detector performance would be improved by increasing the aspect ratio L/W, even though $W\propto I$. However, in dissipative conductors ($R_{xx}\neq 0$), a larger value of L/W increases the background resistance, R_{xx}, as well, which in turn increases the noise power density, $S_\nu=S_N+S_S+S_{1/f}$, where $S_N=4k_BT(R_H+R_{xx})$ with the Boltzman constant, k_B, is the Nyquist's noise, S_S is the Shot noise, the maximum value of which is given by $S_S=2eR_{xx}^2I$ (in the case when the energy relaxation is absent in the conductor),[3] and $S_{1/f}\propto\{(R_{xx}I)^2/(LW)\}(1/f)$ is the $1/f$ noise.[4] A conductor with a large aspect ratio is therefore not necessarily profitable. In contrast, in IQHE Hall bars with vanishing $R_{xx}=0$, the noise power arises only from $S_\nu=S_N=4k_BTR_H$,[3] which remains small regardless of arbitrarily large values of L/W. Hence, the photosignal can be made larger by increasing L/W without the cost of noise increment, and longer IQHE devices can be expected to function as extremely sensitive FIR detectors.

IQHE devices have already been used as sensitive FIR detectors.[5,6] Despite these applications and despite the relatively long history of experimental studies of FIR photoresponse in 2DEG systems at high magnetic fields,[7–10] the mechanism of FIR photoresponse in IQHE devices has not

[a]Also a Research Fellow of the Japan Society for the Promotion of Science; electronic mail: kawano@mujin.c.u-tokyo.ac.jp
[b]Present address: NEC Photonic and Wireless Devices Research Laboratories, 9-1, Seiran 2-chome, Otsu, Shiga 520-0833, Japan.
[c]Present address: NTT Photonics Laboratories, 3-1 Morinosato-Wakamiya, Atsugi, Kanagawa 243-0198, Japan.

been satisfactorily clarified. Experimental studies started in the early 1980s by using gas lasers of fixed wavelengths as the radiation source.[7–10] A nonresonant component of photosignals as well as the CR component of photosignals was found to be present, where the signals existed not only in the vicinity of IQHE plateaus but also in the regions outside the IQHE plateaus,[8–10] which suggested that the resonant signals arise from the effect of electron heating.[8,9] Time-resolved measurements reported the coexistence of fast (<0.1–$10\ \mu$s) and slow (1–30 ms) components of photosignals, where the slow signals were dominated by nonresonant components probably due to an increase in the lattice temperature, T_L.[10] Using a tunable germanium laser,[11] Vasil'ev *et al.* revealed that the resonant photoresponse takes a maximum amplitude at the center of a quantum Hall plateau.[12]

These earlier experiments used Hall bars with small aspect ratios ($L/W=2-5$), which necessitated the application of relatively intense FIR radiation from lasers ($\sim$milliwatts). Hence, the possibility of lattice heating was not ruled out, which complicated the interpretation of the photoresponse mechanism. Recent studies using extremely long Hall bars ($L/W=3\times10^3$) along with weak FIR illumination ($<$milliwatts) revealed that a nonresonant signal is absent and that the resonant response is limited to the close vicinity of IQHE plateaus.[13,14] The spectral photoresponse showed sharp resonance that agrees with the CR absorption lines taken in the transmission measurements.[14] In contrast to the results described by Vasil'ev *et al.* suggesting the maximum photoresponse at exactly the center of IQHE plateaus,[12] the photoresponse under weak excitation featured two prominent peaks, one located on either side of the IQHE plateaus.[13,14] The profile of the peaked structure, $\Delta V_{xx}(B)$, resembled that of the derivative of R_{xx} with respect to T_L, $\partial R_{xx}/\partial T_L$,[13,14] which is consistent with the earlier report[8,9] and supported the effect of electron heating as the mechanism of photoresponse.

Despite these recent experiments, detailed characteristics of the photoresponse have not yet been systematically studied. For instance, the influence of relevant parameters such as L/W, I, electron mobility, and illumination intensity on photoresponse signals has not been studied. Accordingly, we still do not have a clear picture of the mechanism of photoresponse, and we therefore cannot outline firm guidelines for designing better FIR detectors. In this work, we first achieve better understanding of the mechanism behind photoresponse by carrying out systematic studies and then use the information gained to help us design guidelines for constructing improved detectors. We used weak and tunable cyclotron radiation from *n*-type InSb Hall devices as the FIR radiation. The photoresponse does not peak exactly at the center of the IQHE plateaus, but it reaches a maximum slightly outside IQHE plateaus, at magnetic field positions where R_{xx} is small but finite. This is not exactly the condition considered at the beginning of this section, and we will see that the residual R_{xx} can be much larger (a few hundred kiloohms) than the R_H in samples of extremely large aspect ratios ($L/W\sim10^3$). Nevertheless, the characteristic of the IQHE that $\rho_{xx}\ll\rho_{xy}$ remains valid, and the values of residual R_{xx} are still much smaller than the typical impedance ($\gg10\ \mathrm{M}\Omega$) of photoconductive-type or bolometric-type conventional detectors. This makes meandering, long quantum Hall bars low-noise and high-sensitive FIR detectors, as will be described.

It should be mentioned that another class of photoresponse, ascribable to edge states, has been reported on the 2DEG systems in the IQHE regime.[15–17] Nevertheless, we will restrict our discussion in this article to the bulk photoresponse occurring in the interior region of 2DEG layers, because the edge-state related photoresponse is discernible only in lower levels of bias current ($<0.5\ \mu$A) and the relevant photosignal is correspondingly small.

This article is organized as follows. After describing the experimental setup in Sec. II, we present experimental results in Sec. III. In Sec. III A, we describe B dependence of the photoresponse studied on seven different samples. We find two-peaked structures in the vicinity of IQHE regimes. In the following subsections, we study the effects of L/W (Sec. III B), electron-mobility (Sec. III C), bias current (Sec. III D), lattice temperature (Sec. III E), and illumination intensity (Sec. III F) on the photoresponse. In Sec. III C, the recombination lifetime of photoexcited electrons is shown to reach as long a value as 0.6 ms in a high-mobility sample at $T_L=4.2$ K with nonexponential decay of photosignals. We will discuss a multitrapping process of photoexcited carriers between localized states and delocalized states. In Sec. III G, the electrical noise from Hall bars is studied and confirmed to be suppressed in the vicinity of IQHE regimes, which makes IQHE devices sensitive FIR detectors, as is predicted at the beginning of this section. In Sec. III H, we describe preliminary attempts at wavelength tuning of the FIR detection in terms of electron-density variation. Section IV is devoted to interpretation of the mechanism of photoresponse, and we also discuss the performance of IQHE devices as FIR detectors. In Sec. IV A, the photoresponse signal, $\Delta V_{xx}(B)$, is analyzed by considering the experimentally studied recombination lifetime of photoexcited carriers along with the theoretically derived specific heat of 2DEG systems, and the photosignal is shown to result from a rise in the effective electron temperature, ΔT_e. In Sec. IV B, we discuss the development of a fundamental guideline for designing IQHE devices as high-sensitive narrow-band FIR detectors.

II. EXPERIMENTAL SETUP

Samples are Hall bars fabricated on four different GaAs/AlGaAs heterostructure crystals designed as A, B, C, and D, which have a 4.2 K electron mobility ranging from $\mu=80\ \mathrm{m}^2/\mathrm{V\,s}$ to $\mu=11\ \mathrm{m}^2/\mathrm{V\,s}$, as listed on Table I. Only sample A1 is a standard rectangular Hall bar, as illustrated in Fig. 1(a). All the other samples are six-terminal Hall bars with a long 2DEG channel running zigzag in a $4\times4\ \mathrm{mm}^2$ square, as schematically shown in the left panel of Fig. 1(b), and an equivalent electrode geometry is illustrated in the right panel of Fig. 1(b). The ratio of the inter voltage-probe distance L to the width W, L/W, is extremely large in these snake-like devices.

As a tunable source of FIR radiation, we use *n*-type InSb Hall devices 4 mm long, 3 mm wide, and 0.1 mm thick.[18]

TABLE I. Sample characteristics. Values of the 4.2 K-mobility μ, the 4.2 K-electron density n_s, the intervoltage-probe distance L, and the width W of samples.

Sample No.	Crystal	μ (m^2/V s)	n_s (10^{15} m^{-2})	L (mm)	W (μm)	L/W
A1	A	80	2.6	2.5	1500	1.7
A2				66	180	367
A3				167	50	3.3×10^3
A4				224	3	7.5×10^4
B3	B	56	2.5	167	50	3.3×10^3
C3	C	20	3.0	167	50	3.3×10^3
D3	D	11	2.6	167	50	3.3×10^3

When a current (up to 3 mA) is passed through the device in a magnetic field B_E, a relatively broadband ($\Delta v = 20\,\mathrm{cm}^{-1}$) cyclotron radiation centered at the cyclotron frequency $\hbar\omega_c = eB/m_c^*$, with $m_c^* = 0.014m_0$ (m_0: the free electron mass), is emitted owing to the nonequilibrium electron distribution among different Landau levels. The emission band is tunable over a range $\hbar\omega_c = 43-309\,\mathrm{cm}^{-1}$ ($B_E = 0.6-4.3$ T).

The emitter and the sample are placed at the centers of two superconducting solenoids that are located in the same cryostat. The distance between the emitter and the sample is 30 cm. The radiation is guided through a metallic light pipe of a bore 7 mmϕ. The whole system is directly immersed in liquid helium. The intensity of incident radiation at the position of the IQHE sample is lower than 1 nW, which is far smaller than those in the previous studies using lasers.[7–10,12]

Throughout the measurements, a dc-bias current, I_{14}, is passed through contacts 1 and 4 [Figs. 1(a) and 1(b)], and the longitudinal voltage V_{23} between contacts 2 and 3 is studied. The emitter is excited with a sinusoidal ac voltage (±4 V or ±2 mA) at 10 Hz unless otherwise specified, and the modulation signal, $V_{\mathrm{sig}} = \Delta V_{23}$, is recorded with a standard lock-in technique. Most of the measurements are carried out at 4.2 K.

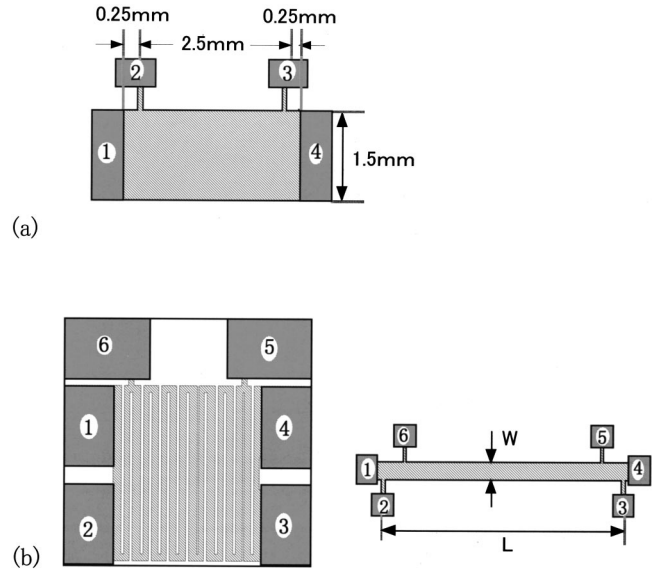

FIG. 1. Schematics of samples. (a) A standard Hall bar, as it was applied in the case of sample A1. (b) A snake-like long 2DEG Hall bar, applying to all the samples except A1. An equivalent geometry is illustrated in the right panel.

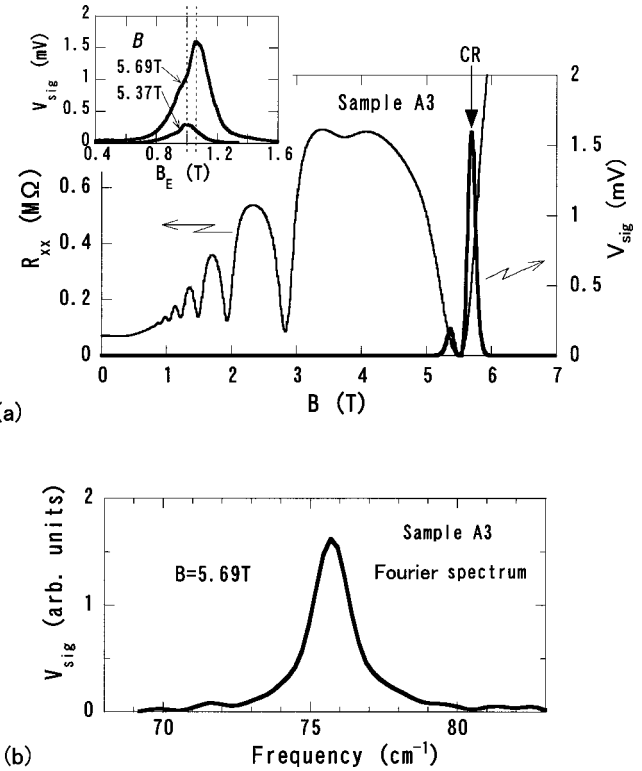

FIG. 2. (a) The FIR photoresponse signal, V_{sig} (the thick solid line), and the longitudinal resistance, R_{xx} (the thin solid line), versus B at $I = 4$ μA in sample A3 at 4.2 K. B_E is fixed at 1.06 T. The inset shows the FIR photoresponse signals in the sweep of B_E, where B is fixed at $B = 5.69$ T and $B = 5.37$ T. The dotted lines indicate the positions, $B_E = 1.00$ T and $B = 1.06$ T, at which the CR is expected for $B = 5.37$ T and $B = 5.69$ T, respectively. (b) The spectrum of the FIR response at $B = 5.69$ T and $I = 4$ μA, studied by a Fourier transform spectrometer with a mercury lamp as the illumination source.

III. EXPERIMENTAL RESULTS

A. Fundamental features

The thick solid line in Fig. 2(a) displays a typical example of FIR response, $V_{\mathrm{sig}} = \Delta V_{23}$, obtained when $B_E = 1.06$ T is applied to the n-InSb emitter. The radiation corresponds to the CR of 2DEG in GaAs in magnetic fields of $B = 5-6$ T (the $v = 2$ quantum Hall plateau). The thin solid line in Fig. 2(a) shows the longitudinal resistance, $R_{xx} = V_{23}/I_{14}$, taken simultaneously at the bias current of $I_{14} = 4$ μA. We note that a large photoresponse emerges on the lower and the higher B sides of the $v = 2$ plateau, forming two prominent peaks. The inset of Fig. 2(a) displays how the amplitudes, V_{sig}, of the higher-B peak ($B_{h\,\mathrm{peak}} = 5.69$ T) and the lower-B peak ($B_{l\,\mathrm{peak}} = 5.37$ T), vary with B_E. The linewidth of the spectra shown in the inset is determined by the relatively broad emission band from the n-InSb device, and it demonstrates that the two-peaked structure of V_{sig} in Fig. 2(a) is not ascribed to the radiation spectra of the n-InSb device but is the genuine characteristic of the FIR response shown by the GaAs IQHE sample.

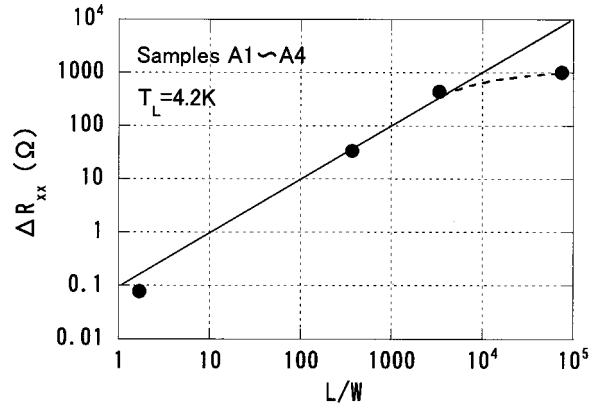

FIG. 3. The FIR photoresponse in terms of the resistance, ΔR_{xx}, as a function of the aspect ratio of Hall bars, L/W. Samples A1–A4 are used. The solid line indicates the linear relation, $R_{xx} \propto L/W$.

As displayed in Fig. 2(b), the true spectral response is sharp, with a full width at the half maximum of $\Delta \upsilon = 1.5\,\mathrm{cm}^{-1}$, where V_{sig} at $B_{h\ \mathrm{peak}} = 5.69\,\mathrm{T}$ is studied with a Fourier transform spectrometer ($\Delta \upsilon = 0.2\,\mathrm{cm}^{-1}$). The linewidth is close to that of the CR absorption line.

Though not shown here, we also observed a large photoresponse due to CR in the vicinity of other quantum Hall plateaus ($\upsilon = 4$ and 6), while no discernible signal emerged in the B ranges away from the quantum Hall plateaus. This is in agreement with previous reports.[13,14] The two-peaked structure of $V_{\mathrm{sig}}(B)$, reported also in Refs. 13 and 14, is a general trend observed in other IQHE plateaus (if they are well developed) and also in other crystals. In the lowest-mobility sample D3, however, the two-peaked structure is modified in such a manner that a prominent V_{sig} peak develops also at the center of the $\upsilon = 2$ plateau as the temperature is lowered to 1.6 K.

B. Aspect ratio of Hall bars

As shown by Eq. (1), ΔR_{xx} should be proportional to the aspect ratio, L/W, of Hall bars if the photoresponse signal is induced by the *resistivity change* $\Delta \rho_{xx}$ ascribable to the *bulk states*. Figure 3 demonstrates this relation, $\Delta R_{xx} \propto L/W$, obtained from the response peak at $B_{h\ \mathrm{peak}}$ in samples A1–A4. The current, I, for each sample ($I = 40$, $I = 15.2$, $I = 4$, and $I = 0.26\,\mu\mathrm{A}$ for A1–A4, respectively) is chosen to be in the range where V_{sig} is proportional to I. Linear dependence, $R_{xx} \propto L/W$, is evident over three orders of magnitude in L/W, confirming that the photoresponse is a bulk phenomenon. We note, however, that the data point of sample A4 with the largest value of $L/W = 7.5 \times 10^4$ falls to a somewhat lower value than the linear extrapolation. This discrepancy is not likely to be a consequence of the large aspect ratio but is probably due to the small width ($W = 3\,\mu\mathrm{m}$) of sample A4, which relates to a detailed kinetics of photoresponse. This is an important issue for designing high-performance detectors and will be discussed in more detail in Sec. IV A.

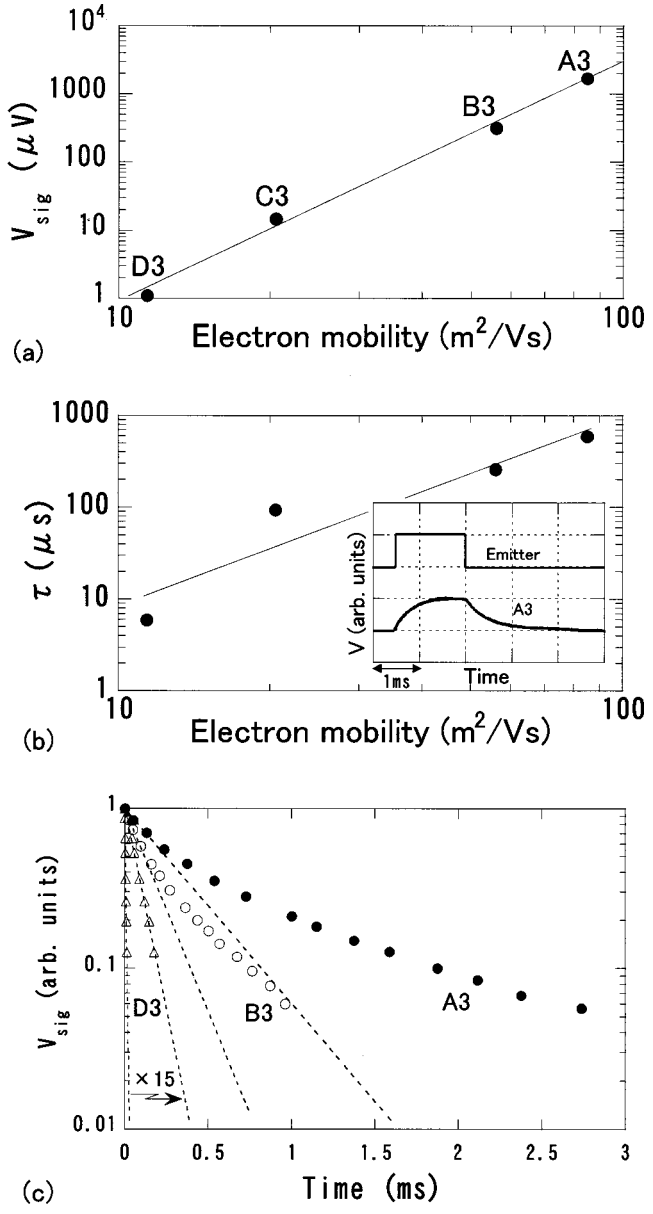

FIG. 4. Electron-mobility dependence of (a) V_{sig} and (b) the characteristic time constant, τ. Samples A3, B3, C3, and D3 are used at $I = 3\,\mu\mathrm{A}$. The magnetic field, B, is fixed at the values where V_{sig} takes on the maximum around $\nu = 2$; viz. $B = 5.69$, 5.35, 6.45, and 5.76 T for A3–D3, respectively. The inset in (b) shows the time trace of the FIR response in sample A3 along with a pulsed wave form of excitation. (c) Time trace of the FIR response after the pulsed excitation on a semi-logarithmic scale; sample A3 (●), sample B3 (○), and sample D3 (△). Values of B and I in respective samples are fixed at the same values as those in Figs. 4(a) and 4(b). As for sample D3, the data points are plotted also on a time scale magnified by a factor of 15. The dotted lines are an extrapolation of the exponential decay in the earlier stage of time traces.

C. Electron mobility

The value of electron mobility crucially affects the amplitude of a FIR response, as shown in Fig. 4(a), where values of V_{sig} at $I = 3\,\mu\mathrm{A}$ in the same-geometry samples A3, B3, C3, and D3, fabricated on different crystals, are plotted against the electron mobility. All the data points indicate the peak value of V_{sig} on the higher-B side of the $\upsilon = 2$ plateau ($B_{h\ \mathrm{peak}} = 5.69\,\mathrm{T}$, $B_{h\ \mathrm{peak}} = 5.35\,\mathrm{T}$, $B_{h\ \mathrm{peak}} = 6.45\,\mathrm{T}$, and $B_{h\ \mathrm{peak}} = 5.76\,\mathrm{T}$ for A3, B3, C3, and D3, respectively). The

value of V_{sig} systematically increases by about three orders of magnitude as the mobility increases by a factor of 8.

As exemplified for sample A3 in the inset of Fig. 4(b), the real-time trace of the photoresponse was studied on all the samples by exciting the n-InSb emitter with a pulsed current of durations 20 μs–5 ms and a rise (fall) time of about 0.1 μs. The speed of the measurement system was about 2 μs, which was fast enough to study the intrinsic FIR response. The characteristic time constant of photoresponse, τ, defined as the time at which V_{sig} decays by the factor e after the end of pulsed illumination, is long, and it remarkably increases when electron mobility is increased, as shown in Fig. 4(b), where values of τ were determined under the same conditions as those for the data points of Fig. 4(a). Note that the corresponding increase of τ accompanying the increase of electron mobility [Fig. 4(b)] is close but not exactly equal to the increment of the signal amplitude V_{sig} [Fig. 4(a)].

The characteristic time constant τ corresponds to the recombination lifetime of excited electron-hole pairs in the upper and the lower Landau levels. The large values of τ (5 μs–0.6 ms at 4.2 K) suggest a multitrapping process of excited electrons (or holes) between localized states and delocalized states in the Landau level, as will be discussed in Sec. II A. This expectation is strengthened by Fig. 4(c), which elucidates the time decay of the photoresponse after the end of pulsed illumination in samples, A3, B3, and D3. We note that the decay curve for the higher-mobility samples, B3 and A3, is not described by a simple exponential function of a single time constant but has long-lived components. In the lowest-mobility sample, D3, however, the decay is described by a simple exponential function. In general, nonexponential decay with long-lived components is a signature of relaxation kinetics in disordered systems,[19] which gives additional support for the model of a multitrapping process.

D. Bias current

Figure 5(a) shows V_{sig} against the bias current I for sample A3 at 4.2 and 1.6 K. For either temperature, plotted are the peak values of V_{sig} at $B_{h\,\mathrm{peak}}$ (white and black circles) and $B_{l\,\mathrm{peak}}$ (white and black triangles) of the $\upsilon=2$ IQHE plateau. At both temperatures, V_{sig} at $B_{h\,\mathrm{peak}}$ linearly increases with I in a small I range, whereas V_{sig} at $B_{l\,\mathrm{peak}}$ increases superlinearly with I without showing linear dependence in any range of I. As I increases further, the increase of V_{sig} at both $B_{h\,\mathrm{peak}}$ and $B_{h\,\mathrm{peak}}$ levels off and starts decreasing. The overall feature is similar between $T_L=4.2$ K and $T_L=1.6$ K, except that the characteristic range of I is expanded to higher values. Similar features are reported by Kawaguchi *et al.*[20]

Let us first note V_{sig} at $B_{h\,\mathrm{peak}}$. We define I_d as the current at which V_{sig} starts decreasing and study values of I_d in samples of different W. The white circles in Fig. 5(b) indicate the data taken in samples A1–A4 at $B_{h\,\mathrm{peak}}$ and are compared with the black circles showing the critical currents, I_c, of the IQHE breakdown *at the center of the* $\upsilon=2$-IQHE *plateau*[21,22] studied in many different Hall bars

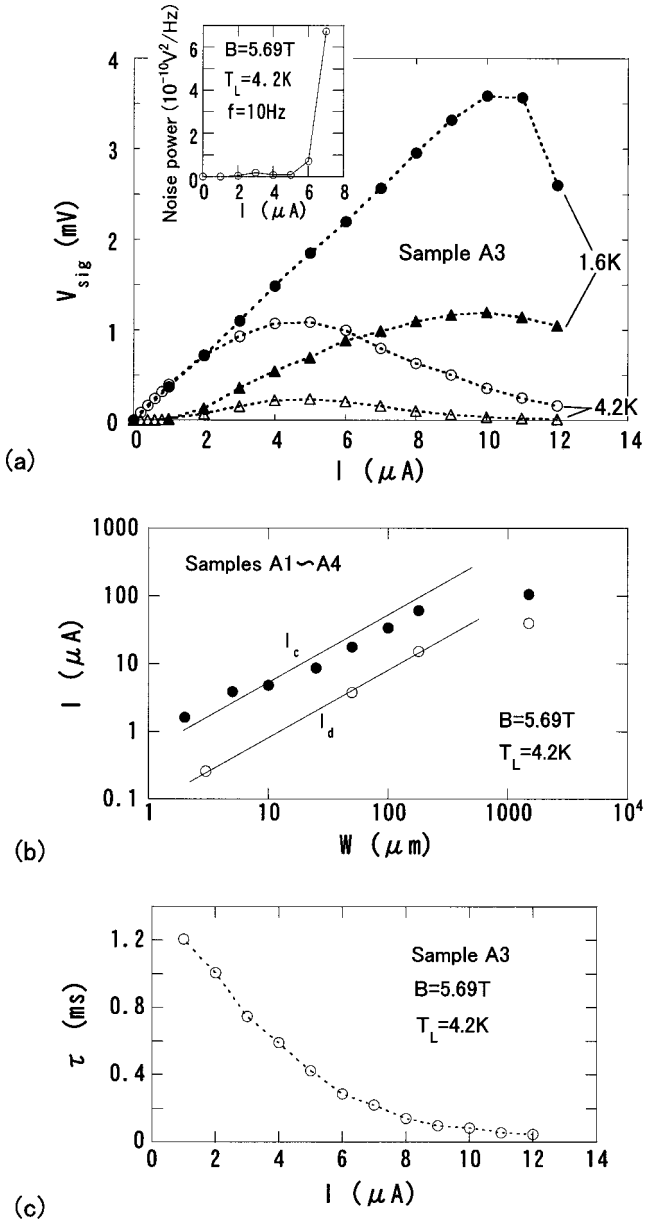

FIG. 5. (a) V_{sig} as a function of the bias current in sample A3, where $B=5.69$ T(●) and $B=5.37$ T(▲) at $T_L=1.6$ K, and $B=5.69$ T(○), $B=5.37$ T(△) at $T_L=4.2$ K. The inset shows the bias current dependence of the noise power at $f=10$ Hz, $B=5.69$ T, and $T_L=4.2$ K. (b) Sample-width dependence of the current, I_d(○), at which V_{sig} reaches the maximum, and the critical current for the IQHE breakdown, I_c(●). (c) Bias current dependence of τ in sample A3 at $B=5.69$ T and $T_L=4.2$ K.

fabricated on the same wafer, A. Values of I_d are systematically smaller than those of I_c, but the W dependence is similar in the two: I_d and I_c increase linearly with W. (The apparent deviation from the W linear dependence in the widest sample of $W=1500$ μm in Fig. 5(b) is not intrinsic to the 2DEG channel but is ascribed to the local breakdown near the current contact).[6] As for the amplitude discrepancy between I_d and I_c, note that $B_{h\,\mathrm{peak}}=5.69$ T at which I_d is determined is shifted from the center of the IQHE plateau, B_{center}, at which I_c is determined. Additional studies confirmed that the critical current of the IQHE breakdown, at which R_{xx} starts to increase rapidly at $B_{h\,\mathrm{peak}}$, is nearly equal

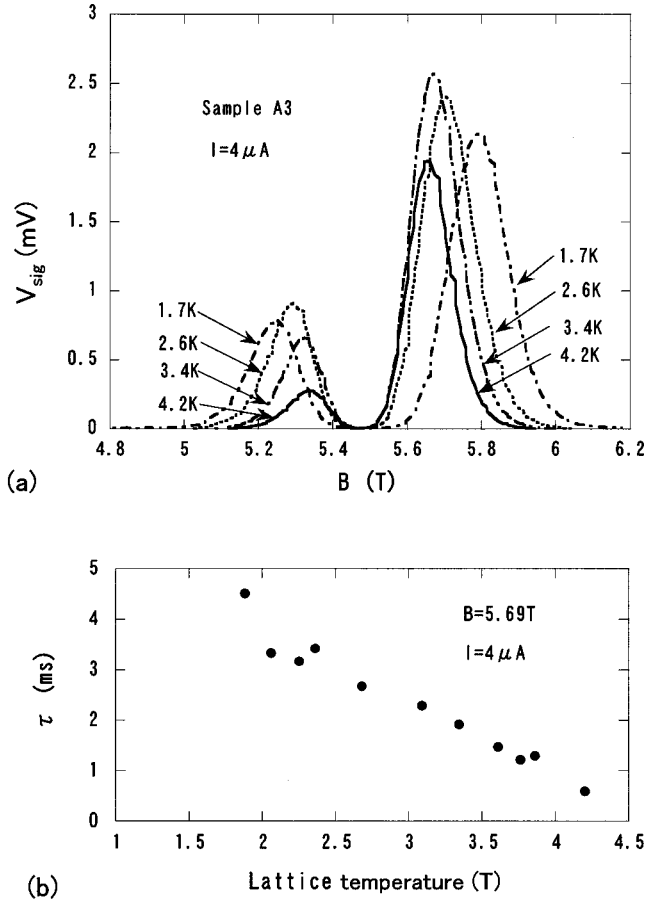

FIG. 6. (a) Two-peaked structure in $V_{sig}(B)$ at different temperatures in sample A3. (b) The characteristic time constant, τ, of the FIR response against the lattice temperature in sample A3 at $B=5.69$ T and $I=4$ μA.

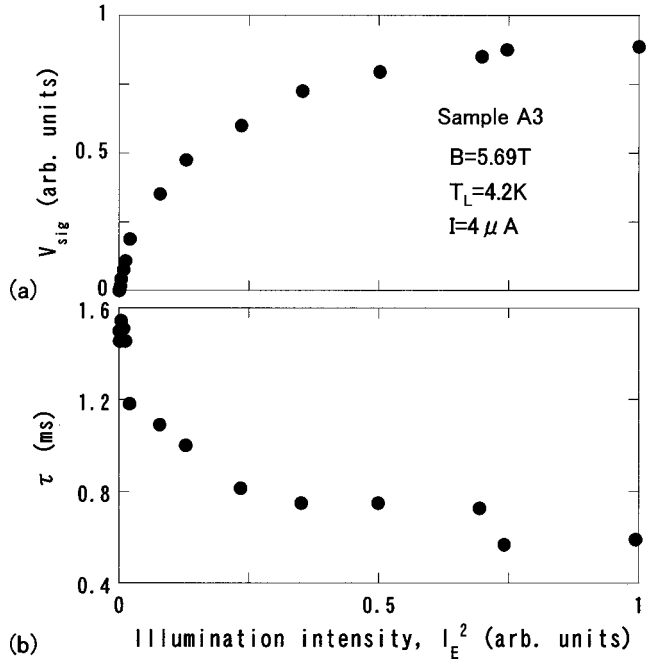

FIG. 7. Dependence of V_{sig} (a) and τ (b) on the illumination intensity at $B=5.69$ T, $T_L=4.2$ K, and $I=4$ μA in sample A3.

to I_d, as may also be expected from the inset of Fig. 5(a), where the noise power is shown against I. The ratio $I_c(B_{\text{center}})/I_d(B_{h\ \text{peak}})$ is found to range from 3 to 6 at 4.2 K, depending on the crystal wafer. Hence, we suppose that the saturation and decrease of V_{sig} with increasing I originate from current-induced heating of 2DEG systems, which probably makes the 2DEG systems insensitive to the CR-induced heating.

The characteristic time constant of photoresponse, τ, in sample A3 at $B_{h\ \text{peak}}=5.69$ T and $T_L=4.2$ K, determined similarly as described earlier, decreases monotonously with increasing current, as shown in Fig. 5(c). The strongly falling τ partly explains the sublinear I dependence of V_{sig} but predicts an even stronger suppression of V_{sig} at larger currents (>5 μA) than those seen in Fig. 5(a).

Let us turn to V_{sig} at $B_{l\ \text{peak}}$ in Fig. 5(a) and note that it is strongly suppressed at low current levels (<1 μA). It is well established experimentally and analyzed theoretically that, in a B range on the lower-B side of a IQHE plateau at low current levels below 1 μA, dissipationless edge channels of lower Landau levels carry a substantial part of the current, and the longitudinal resistivity, ρ_{xx}, arising from bulk states of the topmost Landau level does not yield longitudinal resistance R_{xx}.[23] Since this well-known effect may also apply to the CR-induced $\Delta\rho_{xx}$, we interpret the suppressed amplitude of V_{sig} at low levels of I as a consequence of decoupled edge and bulk states at small I. The superlinear I dependence of V_{sig} ($0.2<I<3$ μA) can be ascribed to the increasing coupling between the edge and bulk states resulting from increasing I.[23] As for the saturation and the decrease of V_{sig} at higher levels of $I(>4$ μA), the mechanism may be the same as that discussed earlier for V_{sig} at $B_{h\ \text{peak}}$.

E. Lattice temperature

The lattice-temperature dependence of V_{sig} in sample A3 in the vicinity of the $\upsilon=2$ IQHE plateau is displayed in Fig. 6(a). The peak positions, $B_{h\ \text{peak}}$ and $B_{l\ \text{peak}}$, gradually shift away from each other as the lattice temperature T_L decreases. The increasing separation is in accordance with the width broadening of the IQHE plateau with lowering T_L. At the fixed current, $I=4$ μA, the peak amplitudes of V_{sig} increase with decreasing T_L down to 3 K but they decrease as T_L is lowered below $\sim$3 K.

Figure 6(b) shows the T_L dependence of the time constant of the photoresponse, τ, studied at $B_{h\ \text{peak}}$. As T_L decreases from 4.2 to 1.7 K, τ rapidly increases, by about one order of magnitude, and reaches 4.5 ms. Though not shown here, τ at $B_{l\ \text{peak}}$ (5.37 T at $T=4.2$ K) exhibits similar behavior. The dependence of the peak value of V_{sig} at $B_{h\ \text{peak}}$ shown in Fig. 6(a) cannot be explained solely by the monotonic behavior of τ shown in Fig. 6(b). This suggest that we need to take other parameters into consideration to understand the amplitude of V_{sig}, as will be discussed in Sec. IV A.

F. Illumination intensity

Figures 7(a) and 7(b) show the amplitude, V_{sig}, and the characteristic time constant, τ, of photoresponse as a function of the illumination intensity for sample A3 at $B_{h\ \text{peak}}$

$=5.69\,\mathrm{T}$ and $I=4\ \mu\mathrm{A}$, respectively. The horizontal scales of the figures are given in terms of the square of the emitter current, I_E^2, which was confirmed to be nearly proportional to the illumination intensity by an additional calibration procedure using a doped-Ge photoconductive detector. The maximum intensity studied (the unity on the scale) corresponds roughly to 10 nW/cm^2 at the place of the sample.

The sublinear dependence of V_{sig} at a lower level of illumination (<3 nW/cm^2) can be accounted for by the corresponding decrease in τ, but the stronger saturation behavior of V_{sig} at a higher level of illumination (>5 nW/cm^2) cannot be ascribed only to the effect of τ. A typical illumination intensity applied for other measurements in the present experiments corresponds roughly to 2 nW/cm^2, or to 0.25 on the scale of Fig. 7. The responsiveness, $V_{\mathrm{sig}}/P_{\mathrm{FIR}}$, of sample A3 determined at the lowest level of illumination intensity is roughly 10^8 V/W.

G. Noise

As the modulation frequency, f, of illumination increases beyond about 100 Hz, the detected signal amplitude starts decreasing in sample A3, as shown in the upper panel of Fig. 8(a). This behavior is probably accounted for by the characteristic time constant, $\tau=0.6\,\mathrm{ms}$, along with components of longer time constants in sample A3.

We studied noise power, $S_V=S_N+S_S+S_{1/f}$, in sample A3 at $B_{h\,\mathrm{peak}}=5.69\,\mathrm{T}$, $I=4\ \mu\mathrm{A}$, and $T_L=4.2\,\mathrm{K}$ in the dark condition (with a 1 Hz bandwidth), shown in the lower panel of Fig. 8(a). The Nyquist's noise, $S_N=4k_BT(R_H+R_{xx})=4.9\times10^{-17}\,\mathrm{V^2/Hz}$, with $R_H=12.9\,\mathrm{k\Omega}$, $R_{xx}=200\,\mathrm{k\Omega}$, and $T_L=4.2\,\mathrm{K}$, and the upper bound of the Shot noise, $S_S=2eR_{xx}^2I=5.1\times10^{-14}\,\mathrm{V^2/Hz}$, are indicated by straight lines for comparison. The measured noise shows a gradual decrease in the range of 10–10^4 3Hz, maintaining a much higher level than S_N. A low frequency range (<100 Hz) is of interest from the application viewpoint because V_{sig} does not suffer from amplitude reduction at $f<100\,\mathrm{Hz}$. In such a low f range, $1/f$ noise, $S_{1/f}$, is likely to dominate. We suppose that the dominant noise primarily arises from generation-recombination electrons between localized states and delocalized states in the presence of current, as suggested by Kil *et al.*[24,25]

Although the noise arises primarily from the finite value of R_{xx} at $B_{h\,\mathrm{peak}}$ (or $B_{l\mathrm{peak}}$), the size of R_{xx} is small and the resultant noise power has been remarkably suppressed owing to the IQHE. This is demonstrated in Fig. 8(b), where S_V at $f=10\,\mathrm{Hz}$ is displayed in the lower panel as a function of B together with the B dependence of V_{sig} in the upper panel. The noise power, S_V, takes a distinct minimum at the center of the $\upsilon=2$ plateau, and the magnetic field positions ($B_{h\,\mathrm{peak}}$ and $B_{l\,\mathrm{peak}}$) at which the FIR response is maximal are close to the plateau center. In a conventional FIR detector, a doped germanium detector for instance, a typical impedance is on the order of 10 MΩ and the noise power is correspondingly large.

The noise power was found to increase roughly at $I^{1.7}$ up to about I_d, above which it abruptly increases as shown in the inset of Fig. 5(a). Note that the rapid growth of the noise

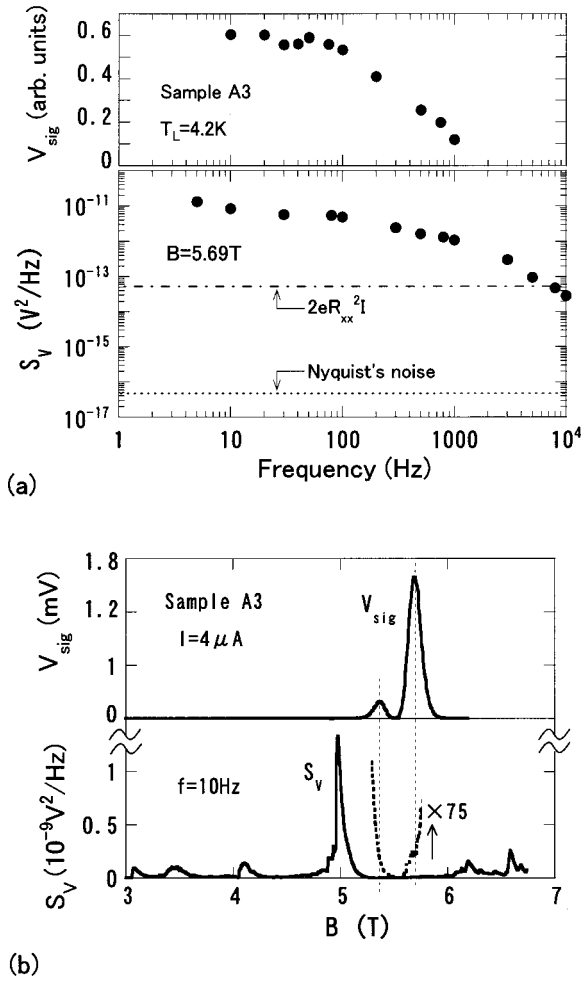

FIG. 8. (a) Dependence of V_{sig} on the excitation frequency (the upper panel) and the noise power spectrum (the lower panel), both taken from sample A3 at $B=5.69\,\mathrm{T}$, $T_L=4.2\,\mathrm{K}$ with $I=4\ \mu\mathrm{A}$. (b) The noise power (the lower panel) at $f=10\,\mathrm{Hz}$ is compared with V_{sig} (the upper panel) in the sweep of B, both taken from sample A3 at $T_L=4.2\,\mathrm{K}$ with $I=4\ \mu\mathrm{A}$.

is accompanied by the decrease in the photoresponse V_{sig}. This, together with the fact that the noise voltage is proportional to $I^{0.85}$ while V_{sig} at $B_{h\,\mathrm{peak}}$ is proportional to I in a lower I range, infers that the best noise performance of the FIR detection will be achieved nearly at $I=I_d$. The noise equivalent power (NEP) of sample A3 is roughly estimated to be $1\times10^{-14}\,\mathrm{W/Hz^{1/2}}$ at $I=I_d$.

H. Tunability

One of the important merits of IQHE detectors is their wavelength selectivity; *viz.* the detected photon energy, $\hbar\omega_c=eB/m^*$, can be tuned by B. In order to fully exploit this property, the electron density, n_s, has to be controlled in accordance with a sweep of B, so that B traces the optimum position for the detection ($B=B_{h\,\mathrm{peak}}$). The variable n_s can be controlled either by applying bias voltages to a metal backgate deposited on the backsurface of a sample substrate or by infrared illumination from a light-emitting diode (LED).

Figure 9 displays preliminary results of FIR detection in conditions of controlled n_s. The sample is fabricated on

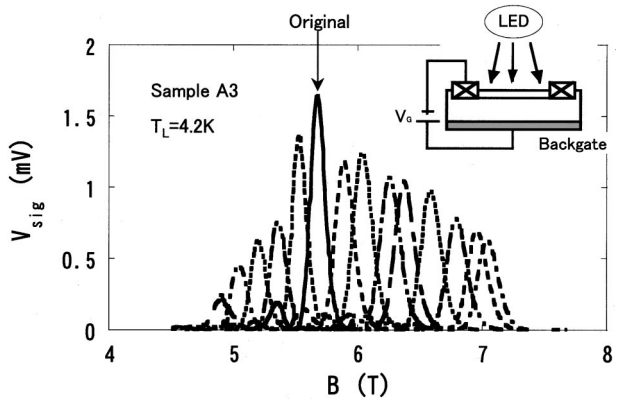

FIG. 9. A series of V_{sig} vs B curves, taken by varying the electron density in sample A3, such as (from the left end to the right end) 1.97, 2.31, 2.38, 2.45, 2.53, 2.60 (for original line), 2.70, 2.76, 2.87, 2.91, 3.02, 3.11, 3.19, and 3.22 (unit: $10^{15}\,m^{-2}$).

crystal A using the geometry of A3, but the substrate is ground to a 200 μm thickness and a metal gate is deposited on the backsurface of the substrate, as illustrated in the inset of Fig. 9. The highest peak at $B=5.69$ T is obtained when n_s is unchanged. Applying a negative gate-bias voltage, V_G, to the backgate decreases n_s and causes the response peak to shift to lower B positions (lower photon energies). A series of different lines located on the lower-B side of the original line corresponds to such reduced values of n_s. The photon energy from the n-InSb emitter is adjusted to yield CR at respective peak positions, and n_s was reduced by about 14% at $V_G=-100$ V. A set of lines drawn on the right higher-B side of the original line is obtained by increasing n_s through LED illumination. The frequency range of FIR detection in Fig. 9 corresponds to 67–97 cm^{-1} (4.9–7 T). We note that the amplitude of V_{sig} decreases either due to application of V_G or due to LED illumination. We do not have a clear interpretation of these effects at present.

IV. DISCUSSION AND INTERPRETATION

In the following sections we interpret the experimental results by considering a mechanism of the FIR response and give some hints for further improving the detector performance.

A. Mechanism

Earlier works reported two components of FIR response: one of a shorter time constant (0.1–10 μs) and the other of a longer time constant (1–30 ms), where the latter was attributed to lattice heating.[8,10,12] In the present experiments, the characteristic time constants of FIR response are relatively large, $\tau=5\,\mu$s–4.5 ms. Nevertheless, the possibility of lattice heating is eliminated due to very low excitation levels applied in the present experiments. This view is supported also by the fact that τ largely depends on various experimental parameters. It is known that the energy relaxation time of inter-Landau-level nonequilibrium electrons is on the order of nanoseconds,[26] where the process is probably dominated by acoustical phonon emissions.[27] Thus, the large values of τ found in the present work, as well as its parameter-sensitive

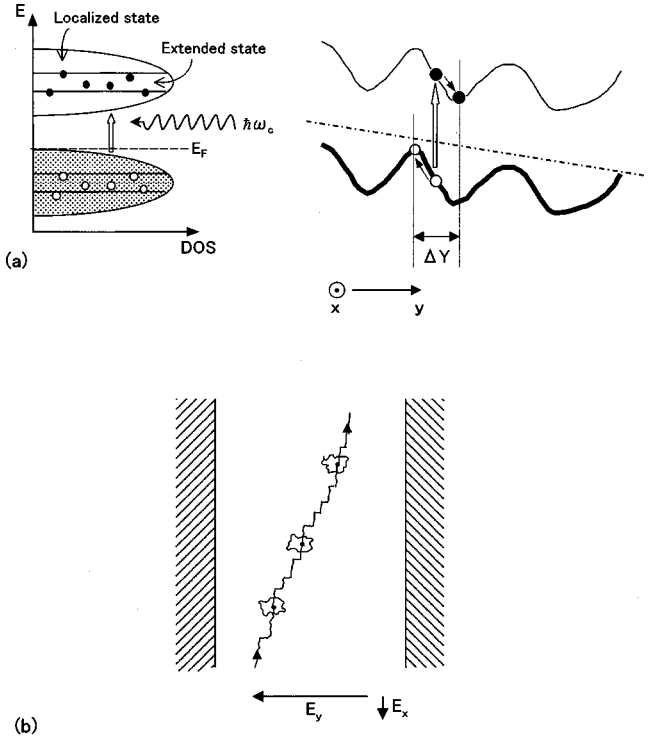

FIG. 10. (a) Schematic representations of Landau-level density of states (on the left) and a Landau-level energy profile (on the right). (b) Schematic illustration of the kinetics of excited electrons drifting in a Hall bar during a multitrapping process.

character, cannot be interpreted in straightforward terms of phonon-related relaxation process and suggest instead that it is necessary to consider the excited-electron kinetics.

There is a long-range disordered potential in 2DEG systems at high magnetic fields. We suppose that the amplitude of the fluctuation potential is large in the close vicinity of the IQHE state, reaching the order of $\hbar\omega_c$ at the exact filling of integer numbers of Landau levels, forming a compressible and incompressible network[28] with a characteristic structure size ΔY.[29] Although the qualitative feature of the network may be substantially unaffected by the cleanness of samples or the electron mobility, the potential fluctuation will be slower in a space yielding larger values of ΔY in higher-mobility samples. Recent studies[30] definitely show that fluctuations of a long range ($\Delta Y=0.04$–$0.2\,\mu$m) are present in high-mobility GaAs systems, values much larger than the magnetic length $l_B=(\hbar/eB)^{1/2}$. Thus, in the 2DEG the local electric field is expected to fluctuate to a typical amplitude of $|E_{\text{fluctuation}}|=\hbar\omega_c/(e\Delta Y)=(3-15)\times10^4$ V/m. This may be true in any real physical 2DEG systems in the vicinity of IQHE states. Note that this fluctuation largely exceeds the average Hall electric field, $E_y=R_H I/W\sim10^3$ V/m, in a condition of $I=I_d$. The average longitudinal electric field, E_x, is much smaller than E_y, where $E_x/E_y=(R_{xx}/R_H)(W/L)=(0.1-1)\times10^{-2}$ at $B_{h\,\text{peak}}$ or $B_{l\,\text{peak}}$.

Figure 10(a) schematically shows a Landau-level density of states (on the left) and a Landau-level energy profile on the cross section of a Hall bar (on the right). The long-range potential fluctuation is superposed on a much slower constant slope of the Hall potential (E_y). The transport current

density, j_d, averaged over a range larger than ΔY points to the x direction in the dark condition. After the process of CR excitation, the majority of excited electrons and holes will rapidly recombine within a short time period, τ_R, by emitting acoustical phonons,[31] where we assume $\tau_R \sim 10$ ns for the recombination lifetime. Although this initial process yields a finite FIR response proportional to τ_R per each excited carrier, its contribution is thought to be unimportant because τ_R is short.

It is important to note that a small number of electrons and holes may escape such a rapid recombination process and eventually fall into (climb up to) localized states formed around local minimum (maximum) potentials, as schematically shown on the right of Fig. 10(a). This relaxation process will occur either via emission of acoustical phonons or energy exchange with other cold electrons. Once trapped at localized states, the electrons and holes will have a distinctly longer recombination lifetime because they are separated by a large distance, $\Delta Y \gg l_B$. The localized electrons (holes) may be occasionally re-excited to delocalized states near the level center, gaining energies from other excited carriers. Once delocalized, the electrons (holes) drift not only in the lengthwise x direction but also in the widthwise y direction, as illustrated in Fig. 10(b). This y drift motion of the excited electrons (holes) leads to dissipation and the FIR response, More accurately, the transient photocurrent (in the y direction) induces a pileup charge along the edges of the Hall bar and causes E_x to develop until the total transport current density points exactly to the x direction, establishing a steady state. Such drift motion of an excited electron (hole) will be interrupted by a recapture process at localized states, but the re-excitation process as described earlier will repeat until the electron (hole) finally recombines with a hole (electron). The FIR response in the present experiments is likely to be ascribed to such a multitrapping. The time constant of a FIR response, τ, is the total lifetime of an electron (hole) including the multitrapping process, while the amplitude of response is proportional to the fractional time, τ_d, that an electron (hole) spends in delocalized states. If we simply assume that the fraction r of the total excited electrons (holes) exerts such a multitrapping effect, its steady state contribution to the FIR response is proportional to $r\tau_d$ per each excited carrier, which is expected to be much larger than the contribution, $(1-r)\tau_R$, from those electrons (holes) that have recombined promptly after the excitation process.

In the following discussion, we will consider only those electrons (holes) that escape the rapid initial recombination process. In the present experimental condition, where the lattice temperature and the excitation level are both sufficiently low, the electrons (holes) will spend most of their life at rest in localized states ($\tau \gg \tau_d$). Hence, τ may be closely linked to the recombination lifetime that electrons (holes) would have if they were in localized states separated by the characteristic distance, ΔY. Most simply, therefore, the recombination probability may be suppressed by the factor[32]

$$1/\tau = A \exp\{-(\Delta Y/l_B)^2\}, \tag{2}$$

due to a small overlapping between the electron and hole wave functions. Since the recombination is more probable when the carriers are in delocalized states, we expect prefactor A in Eq. (2) to be an increasing function of τ_d. The value of ΔY is expected to increase with increaseed electron mobility, while $\Delta Y/l_B \gg 1$ in all the present experimental conditions.

We can interpret several experimental findings in terms of the model just described. First, the recombination rate is strongly suppressed by the factor $\exp\{-(\Delta Y/l_B)^2\}$, accounting for large values of τ. Second, a relatively small change in ΔY can lead to largely different values of τ. Especially, larger values of ΔY in higher-mobility samples tend to yield remarkably larger values of τ, as seen in Fig. 4(b). Third, there must be a finite distribution of ΔY in a given sample, which makes the decay of the FIR response deviate from a simple exponential function, as seen in Fig. 4(c). Fourth, localized states at the sites of local maximum (minimum) potentials will be increasingly occupied and less available for excited electrons (holes) as the excitation level increases. The decrease of τ with increased illumination intensity [Fig. 7(b)] can be ascribed to this effect. Fifth, re-excitation of electrons (holes) to delocalized states will be promoted as the lattice temperature, T_L, is elevated, which causes prefactor A in Eq. (2) to increase with T_L. This will decrease τ as T_L is elevated but will not equally decrease $V_{\rm sig}$, because $V_{\rm sig}$ is affected by τ_d. This is consistent with the features shown in Figs. 6(a) and 6(b). Finally, increasing the bias current, I, will lead to smooth heating of the electron system[33] as well as to partial delocalization of electron states.[34] Both effects may function to increase τ_d and to decrease τ, providing a reasonable account for the I dependence of τ and $V_{\rm sig}$ in Figs. 5(a) and 5(c).

We suggest below an alternative and simple view of the FIR response. The long recombination lifetime of excited carriers leads us to assume that the energy exchange among electrons is significant enough to establish the effective electron temperature $T_e = T_L + \Delta T_e$ and that the CR absorption causes T_e to increase by ΔT_e. The photoresponse signal ΔR_{xx} is then expressed as

$$\Delta R_{xx} = (\partial R_{xx}/\partial T_L)\Delta T_e, \tag{3}$$

where

$$\Delta T_e = P\tau/C_{\rm el}. \tag{4}$$

Here $P = P_{\rm FIR}/(LW)$ is the energy absorption rate per unit area, $C_{\rm el}$ is the 2DEG specific heat per unit area, and τ is the lifetime of photoexcited carriers that is identical to the time constant of the FIR response. For a quantitative estimate, the factor r should be multiplied by the right-hand side of Eq. (4) because the equation refers to the fraction r of the total excited carriers. In fact, the experimentally observed amplitude of the FIR response (Fig. 7) indicates $\Delta T_e \sim 1.7$ mK at $P = 0.1$ nW/cm^2, whereas Eq. (4) with relevant parameter values ($\tau = 0.6$ ms and $C_{\rm el} = 3.4 \times 10^{-14}$ J/K cm^2) derives $\Delta T_e \sim 2$ K, which suggests $r \sim 10^{-3}$.

Next, we discuss the shape of the ΔR_{xx} vs B curve, which is substantially independent of the factor r. Figure 11(a) shows experimental values of $\partial R_{xx}/\partial T_L$ (the thin solid line) and τ (the black dots connected with a dotted line) studied in sample A3 at 4.2 K. We find that τ decreases

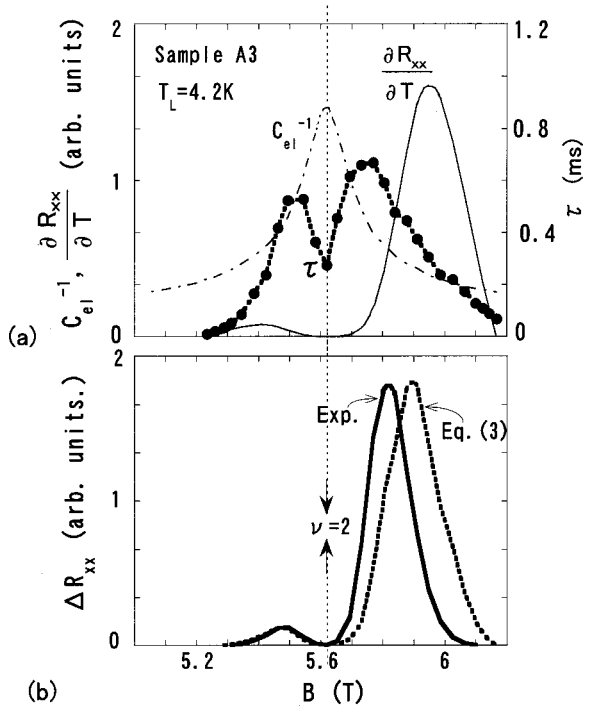

FIG. 11. Analysis of the two-peaked structure of $V_{\rm sig}(B)$ around the $\nu=2$ IQHE plateau. (a) Experimental values of $\partial R_{xx}/\partial T$ (the solid line) and τ (the circles connected with the dotted line), and calculated values of the inverse of the 2DEG heat capacity (the dash-dot line). (b) Experimental values of $V_{\rm sig}(B)$ (the solid line) compared with theoretical values (the broken line) predicted from the three values indicated in Fig. 11(a) through Eq. (3).

rapidly as B departs from the IQHE plateau region ($B<5.2\,\mathrm{T}$ and $B>6.3\,\mathrm{T}$). This is probably because disordered potentials are effectively screened to make delocalization of photoexcited carriers feasible in the B ranges outside the IQHE plateau region. The dash-dot line in Fig. 11(a) shows theoretical values of $C_{\rm el}^{-1}$ which are derived by assuming a Gaussian-type density of states with the level broadening parameter of 0.5 meV and a 5% constant background density of states.[35,36] The dotted line in Fig. 11(b) indicates the values of Eq. (3) obtained by substituting $\partial R_{xx}/\partial T_L$, τ and $C_{\rm el}^{-1}$ with the values shown in Fig. 11(a). The line nicely reproduces the experimental line shape (the solid thick line).

We conclude that the electron-heating model is likely to give a reasonable basis for understanding the FIR response. The fact, observed in our experiment, that a large $V_{\rm sig}$ is observable only in the vicinity of IQHE plateaux is attributed to the remarkable feature of τ that it takes distinctly larger values there as well as to the fact that $C_{\rm el}$ is remarkably smaller in the IQHE plateau region. The two-peaked structure of $V_{\rm sig}(B)$ is primarily ascribed to a similar structure in $\partial R_{xx}/\partial T_L$: namely, $R_{xx}(B)$ sharply rises at the opposite two edges of the IQHE plateau [Fig. 2(a)], and the experimental curve of $\partial R_{xx}/\partial T_L$ vs B forms two prominent positive peaks at these edges, as shown in Fig. 11(a). The separation between the two peaks of $V_{\rm sig}(B)$ decreases with increasing T_L, as shown in Fig. 6(a). This is a consequence of a narrowing of the IQHE plateau region with increasing T_L.

We want to mention that the two-peaked structure of $V_{\rm sig}(B)$ is, strictly, not a general feature, but a feature observable only when the relevant IQHE plateau is well developed. The width of an IQHE plateau decreases until it vanishes as T_L increases to reach a sufficiently high value, roughly about 8 K at $B=5-6\,\mathrm{T}$. It follows that the two peaks in the curve of $\partial R_{xx}/\partial T_L$ vs B merge to form a single peak at a relatively high T_L or a relatively low B. There are three relevant experiments to describe with respect to this feature. Gavrilenko *et al.* and Antonov *et al.*[37] have found that the two-peaked structure of $V_{\rm sig}(B)$ in a higher-B range (>3 T) is indeed replaced by a single-peaked structure ($\nu=6$, 8, 10,...) in a lower-B range (<2 T) at $T_L=4.2\,\mathrm{K}$. Similarly, Vasil'ev *et al.*[12] reported a single-peaked $V_{\rm sig}(B)$ under pulsed intense FIR laser illumination exactly at $\nu=2$, although the IQHE plateau was well developed at $B=5.4\,\mathrm{T}$ and $T_L=4.2\,\mathrm{K}$. We speculate that the pulsed illumination in these experiments was so strong as to heat the electron system to a level of a vanishing IQHE plateau. More recently, Kawaguchi *et al.*[20] reported that the two-peaked structure of $V_{\rm sig}(B)$ changes to a single-peaked structure as the current I increases to enter the breakdown regime of IQHE ($I>I_c$), which is reasonably interpreted as a consequence of a substantial increase in T_e in the breakdown regime.[38]

B. Detector performance

The sensitivity in terms of the NEP achieved in the present work is roughly $\mathrm{NEP}\sim 1\times10^{-14}\,\mathrm{W/Hz^{1/2}}$ with $\sim10^8$ V/W in sample A3 at 4.2 K, where the frequency response is limited to $f\sim300\,\mathrm{Hz}$. The sensitivity is among the highest levels achieved by existing FIR photoconductive detectors. In order to further improve the detector performance, we note here a few points and discuss them briefly. As a general trend, the sensitivity will be higher if detectors are fabricated on higher-mobility crystals, but the speed of the detector will be reduced [Figs. 4(a) and 4(b)].

Let us first figure out the optimum aspect ratio, L/W, in the condition when the detector size or LW is given. The largest applicable current is proportional to W and written as $I_d=CW$, where C is a geometry-independent but crystal-specific constant. Equation (1) shows that $V_{\rm sig}=CL\Delta\rho_{xx}$ when $I=I_d$ is passed thorough the detector. It follows that higher values of L/W are profitable, as already discussed in the introduction of this article. However, there is a restriction as follows: Remember that photoexcited carriers drift not only along the lengthwise direction of a Hall bar but also in the widthwise direction due to scattering events, as illustrated in Fig. 10(b). The distance over which excited carriers travel in the width wise direction during the lifetime should not exceed W. Otherwise, a substantial fraction of photoexcited carriers reach one boundary of the Hall bar traversing the full width, and stop contributing to $V_{\rm sig}$. We interpret the deviation of ΔR_{xx} in sample A4 from the linear dependence in Fig. 3 as a consequence that the travel distance is limited to W of this narrowest sample ($W=3\,\mu\mathrm{m}$) rather than as a direct effect of the aspect ratio, $L/W=7.5\times10^4$. Hence, we suggest that W should be larger than an allowable limit, $W_{\rm min}$, which we roughly set at $W_{\rm min}\sim20\,\mu\mathrm{m}$ in high-mobility samples ($>50\ \mathrm{m^2/V\,s}$).

Let us next ask the optimum size or length, L, of the detector if W is chosen to be the minimum, $W=W_{\min}$. We reduce the size (L) of the detector while focusing the incident illumination, so that the total FIR power absorbed by the detector is kept unchanged. In this case, the illumination power density increases as $L^{-1.0}$, and $V_{\rm sig}=CL\Delta\rho_{xx}$ is kept unchanged because the increase of $\Delta\rho_{xx}\propto L^{-1.0}$ compensates the reduction in L. We expect that the noise voltage will be reduced as $L^{1/2}$ with decreasing L because the $1/f$ noise is predominant in our detectors, for which the noise power is empirically given as $S_{1/f}\propto\{(R_{xx}I)^2/(LW)\}(1/f)\propto L$.[4] We accordingly expect NEP$\propto L^{1/2}$. Hence, the detector size should be minimized to the limit reached by the efficient focusing of incident FIR radiation. The resolution limit in the geometrical optics is given by the wavelength of radiation, which is given by $\lambda_{\rm sub}=\lambda/n$ in a substrate of the refractive index $n=3.57$ (GaAs).

Finally, we would like to include some practical comments about the geometry of optics. In the present experiments, the FIR radiation is incident on the front surface of the substrate, where the 2DEG layer is located only about 0.1 μm below the front surface of the dielectric medium (GaAs). This is not the optimum geometry.[39] We have confirmed in additional measurements that the efficiency of absorption is improved by about a factor of 4 when the radiation is incident from the backside of the substrate. If FIR is incident from the front side, similar improvement will result if the surface is covered with an additional dielectric (pure Si or GaAs).

The sample geometry studied in the present work is far from optimum from the viewpoint of the discussion in this article. We suppose that NEP$\sim 10^{-16}\,\mathrm{W\,Hz^{-1/2}}$ at 4.2 K can be achieved through further improvements in the future.

V. SUMMARY

We have studied the CR-induced FIR photoresponse of 2DEG systems in GaAs/AlGaAs heterostructures at high magnetic fields. In the sweep of a magnetic field, a strong FIR response occurs only in the vicinity of IQHE states, with a two-peaked structure where each peak is located at the edge of an integer quantum Hall plateau. The peak amplitude of the response signal, $V_{\rm sig}$, increases remarkably with increased electron mobility, μ, of samples. The characteristic time constant of the FIR response, τ, which is approximately several microseconds at 4.2 K in a relatively low-mobility sample ($\mu=11\,\mathrm{m^2/V\,s}$), increases largely as μ increases, reaching several hundred microseconds in a sample of $\mu=80\,\mathrm{m^2/V\,s}$. The time trace after pulsed excitation shows a nonexponential decay with longer tails in high-μ samples ($\mu>50\,\mathrm{m^2/V\,s}$). These features suggest a multitrapping process, in which excited electrons and holes in Landau levels repeat the process of being captured by localized states and re-excitation to delocalized states until they finally recombine with each other. The larger photoresponse in higher-μ samples may arise from the longer recombination lifetime that is a consequence of larger separation between excited electrons and holes in smoother impurity potentials. The line shape of the two-peaked structure of the response in the sweep of a magnetic field is accounted for by assuming that the effective electron temperature is raised by the CR absorption. The absence of a strong FIR response in the magnetic field ranges well away from the IQHE states is ascribed to remarkably shorter recombination lifetimes (confirmed by measurements) as well as to a distinctly larger specific heat of the 2DEG (calculated) in such transition regions between the IQHE states.

The highest detector sensitivity achieved is NEP$\sim 1\times10^{-14}\,\mathrm{W/Hz^{1/2}}$ with a voltage responsivity $\sim 10^8$ V/W obtained in an extremely long Hall bar with the aspect ratio of $L/W=3.3\times10^3$ ($W=50\,\mu$m) fabricated on a high-mobility crystal ($\mu=80\,\mathrm{m^2/V\,s}$). IQHE Hall bars may be used as narrow-band and tunable detectors by varying the electron density to cover a frequency range of 67–97 $\mathrm{cm^{-1}}$. Finally we have discussed further possible improvements.

[1] K. von Klitzing, G. Dorda, and M. Pepper, Phys. Rev. Lett. **45**, 494 (1980).
[2] S. Kawaji and J. Wakabayashi, in *Physics in High Magnetic Fields*, edited by S. Chikazumi and N. Miura (Springer, Berlin, 1981), p. 284.
[3] M. Büttiker, Phys. Rev. Lett. **65**, 2901 (1990).
[4] M. B. Weissman, Rev. Mod. Phys. **60**, 537 (1988).
[5] Y. Kawano, Y. Hisanaga, and S. Komiyama, Phys. Rev. B **59**, 12537 (1999).
[6] Y. Kawano and S. Komiyama, Phys. Rev. B **61**, 2931 (2000); Y. Kawano and S. Komiyama, Physica E (Amsterdam) **7**, 502 (2000).
[7] J. C. Mann, Th. Englert, D. C. Tsui, and A. C. Gossard, Appl. Phys. Lett. **40**, 609 (1982).
[8] D. Stein, G. Ebert, K. von Klitzing, and G. Weiman, Surf. Sci. **142**, 406 (1984).
[9] R. E. Horstman, E. J. vd. Broek, and J. Wolter, Solid State Commun. **50**, 753 (1984).
[10] M. J. Chou, D. C. Tsui, and A. Y. Cho, *Proc. of 18th Int. Conf. Phys. of Semicond.* (World Scientific, Stockholm, 1986), p. 437.
[11] As a review, see for example, Opt. Quantum Electron. **23** (1991).
[12] Y. B. Vasil'ev, S. D. Suchalkin, Y. L. Ivanov, P. S. Kop'ev, and I. G. Savel'ev, JETP Lett. **56**, 377 (1992).
[13] S. Komiyama, Y. Kawano, and Y. Hisanaga, Proc. of 21st Int. Conf. on IR&MM Waves BT2, Berlin, 1996.
[14] K. Hirakawa, M. Endo, K. Yamanaka, Y. Hisanaga, and S. Komiyama, *Proc. of 23rd Int. Conf. Phys. of Semicond.* (World Scientific, Berlin, 1996), p. 2543.
[15] E. Dießel, G. Muller, D. Weiss, K. von Klitzing, and G. Weimann, Appl. Phys. Lett. **58**, 2231 (1991).
[16] R. Merz, F. Keilmann, R. J. Haug, and K. Ploog, Phys. Rev. Lett. **70**, 651 (1993).
[17] A. Lorke, J. P. Kotthaus, J. H. English, and A. C. Gossard, Phys. Rev. B **53**, 1054 (1996).
[18] G. Bauer, M. Overhamm, P. Grosse, W. Muller, E. Gornik, and H. W. Potzl, Phys. Status Solidi B **75**, 543 (1976).
[19] For example, J. E. Gloub, S. D. Baranovskii, and P. Thomas, Phys. Rev. B **55**, 4575 (1997).
[20] Y. Kawaguchi, K. Hirakawa, M. Saeki, and S. Komiyama, Proc. of 7th Int. Conf. THz Electronics, Nara, Japan, 1999, p. 229.
[21] G. Ebert, K. von Klitzing, K. Ploog, and G. Waiman, J. Phys. C **16**, 5441 (1983); M. E. Cage, R. F. Dziuba, B. F. Field, E. R. Williams, S. M. Girvin, A. C. Gossard, D. C. Tsui, and R. J. Wagner, Phys. Rev. Lett. **51**, 1374 (1983).
[22] S. Komiyama and Y. Kawaguchi, Phys. Rev. Lett. **77**, 558 (1996); S. Komiyama and Y. Kawaguchi, Phys. Rev. B **61**, 2014 (2000).
[23] S. Komiyama, H. Nii, M. Ohsawa, S. Fukatsu, Y. Shiraki, R. Itoh, and H. Toyoshima, Solid State Commun. **80**, 157 (1991); H. Nii, S. Komiyama, S. Fukatsu, Y. Shiraki, R. Itoh, and H. Toyoshima, Surf. Sci. **263**, 275 (1992); S. Komiyama and H. Nii, Physica B **184**, 7 (1993).
[24] A. J. Kil, R. J. J. Zijlstra, P. M. Koenraad, J. A. Pals, and J. P. Andre, Solid State Commun. **60**, 831 (1986).
[25] A. J. Kil, R. J. J. Zijlstra, M. F. H. Schuurmans, and J. P. Andre, Phys. Rev. B **41**, 5169 (1990).

[26] S. Komiyama *et al.*, Solid State Commun. **54**, 479 (1985).
[27] P. A. Russell, F. F. Ouali, N. P. Hewett, and L. J. Challis, Surf. Sci. **229**, 54 (1990); Fal'ko *et al.*, J. Phys.: Condens. Matter **5**, 3945 (1993).
[28] J. P. Eisenstein, H. L. Stormer, V. Narayamanamurti, A. Y. Cho, and A. C. Gossard, Surf. Sci. **170**, 271 (1986); E. Gornik, R. Lassing, and G. Strasser, *ibid.* **170**, 277 (1986); D. Weiss, E. Stahl, G. Weimann, K. Ploog, and K. von Klitzing, *ibid.* **170**, 285 (1986); R. R. Gerhardts, and V. Gudmundsson, Phys. Rev. B **34**, 2999 (1986).
[29] D. B. Chklovskii, B. I. Shklovskii, and L. I. Glazman, Phys. Rev. B **46**, 4026 (1992).
[30] S. H. Tessmer, P. I. Glicofridis, R. C. Ashoori, L. S. Levitov, and M. R. Melloch, Nature (London) **392**, 51 (1998).
[31] S. Roshko, W. Dietsche, and L. J. Challis, Phys. Rev. Lett. **80**, 3835 (1998).
[32] See, for example, S. Komiyama, H. Hirai, M. Osawa, and Y. Matsuda, Phys. Rev. B **45**, 11085 (1992).
[33] The electron heating effect here should be distinguished from the *bootstrap-type electron heating* that causes breakdown of the IQHE (see Ref. 22).
[34] O. Heinonen, P. L. Taylor, and S. M. Girvin, Phys. Rev. B **30**, 3016 (1984).
[35] E. Gornik, R. Lassing, G. Strasser, H. L. Stormer, A. C. Gossard, and W. Wiegmann, Phys. Rev. Lett. **54**, 1820 (1985).
[36] W. Zawadzki and R. Lassing, Solid State Commun. **50**, 537 (1986).
[37] V. I. Gavrilenko, I. V. Erofeeva, N. G. Kalugin, A. L. Korotkov, M. D. Moldavskaya, Y. Kawano, and S. Komiyama, Proc. of 6th International Symposium Nanostructures: Physics and Technology, St. Petersburg, Russia, June, 1998, p. 497; A. V. Antonov *et al.*, Proc. of International Symposium on Compound Semiconductors-25, Nara, Japan, 1998.
[38] S. Komiyama and Y. Kawaguchi, Phys. Rev. B **61**, 2014 (2000).
[39] *Millimeter Components and Techniques II ''Infrared and millimeter waves,''* edited by K. J. Button (Academic, New York, 1983), Chap. 1.